Feasibility study of an active infrared scanning system for thermal detection of buried antipersonnel landmines. Part I: a basic theoretical approach.

MARCO BALSI[a], MASSIMO CORCIONE[b] and PIERPAOLO DELL'OMO[b]
[a] Dipartimento di Ingegneria Elettronica
[b] Dipartimento di Fisica Tecnica
University of Rome "La Sapienza", via Eudossiana 18
00184 Rome, Italy

Abstract: A new method for thermal sensing of buried anti-personnel landmines aimed at humanitarian de-mining is discussed. The detection system is based on a focused radiant heat source which scans the ground followed by a contactless thermometer. In fact, as heat transfer properties of landmines generally differ from those of the surrounding soil, anomalies in surface temperature distribution may possibly arise owing to the presence of mine candidates. The performance of the method proposed is evaluated by a finite-difference numerical analysis of the time-evolution of the temperature field over the ground investigated, as a result of the absorption of the radiant energy delivered to the soil surface and of its diffusion underneath. Simulations are carried out through a specifically developed time-implicit computer code, for a wide variety of values of the heating power, of the size and shape of the irradiation area, of the scanning speed, and of the burial depth of the landmine. Among the several results obtained, it is found that the amplitude of the thermal anomaly detectable over the ground surface increases linearly with the amount of radiant energy absorbed per unit area, while decreasing exponentially with the burial depth of the landmine.

Keywords: Antipersonnel landmines; Thermal detection; Active scanning; Numerical simulation.

1 Introduction

Antipersonnel landmines cause death and injuries long after a conflict has finished, disrupt local economy, and prevent return of the population affected to normal life and use of the land. United Nations estimate that 110 million landmines have been laid worldwide, and 150 million stocked, while less than 100,000 are being found and destroyed each year. This makes research on more reliable and fast methods for mine detection and clearance very urgent.

Antipersonnel mines (APM) are small, often less than 10cm across, and contain almost no metal. They are normally laid randomly on the ground surface, and are successively displaced and buried by the action of atmospheric phenomena.

Humanitarian de-mining, which our attention is devoted to, is performed after conflicts have ended, often after several years, in order to restore the territory to civil use, aiming at 100% clearing of all mines. Currently used methods for humanitarian de-mining are not satisfactory, as they involve significant risks for deminers, and are very slow, expensive, and not sufficiently reliable [1,2]. Conventional mine-location methods include visual inspection, metal detectors, sniffer dogs, and manual probing.

Emerging mine-location technologies include acoustic stimulation in connection with Doppler laser vibrometers or radars, active electromagnetic methods, natural and artificial gas sensors, neutron excitation, and infrared thermal detection, which is one of the most promising detection method for efficiency and availability of equipment.

The basic principle underlying thermal detection of mines is the difference in thermal conduction properties of explosives with respect to the soil, which causes a temperature difference to appear on the ground surface over a buried mine with respect to other areas when the surface is naturally or artificially heated and/or cooled [3−8]. Thermal detection of mines has the advantage of being sensitive to the bulk material of the mine regardless of its metal content, and of employing quite simple and safe stimulation, either by sunlight, or by lamps, microwave heaters, and hot water. Images of the ground surface are commonly taken by an infrared camera at different times during the heating or cooling process, revealing temperature differences of the order of 0.1K. The main drawback of existing thermal methods is the long time required. Moreover, temperature contrast is rather low, of the order of some tenths of degree, which is close to infrared cameras sensitivity, so that the images

obtained are noisy and require complicated post-processing. The cameras themselves are rather expensive and not easily serviceable, and the interface to the operator is not always simple and intuitive.

In this framework a new concept for thermal antipersonnel mine detection, based on high-flux local irradiation and pointwise surface temperature scanning, is here proposed and discussed.

2 Basic structure of the detection device

The basic structure of the mine detection device proposed here is composed of a focused heater and a contactless thermometer, mounted on a suspended holder that progressively scans the ground surface under examination [9]. The heater delivers infrared power to a small area, having dimensions comparable to those of a typical anti-personnel landmine. The absorption of the thermal stimulation delivered to the soil surface produces a rapid increase in temperature, which is followed by an exponential decay by heat diffusion underneath and heat transfer to the environment. When an object with thermal conduction properties different from those of the background is present, the rates of increase and successive decrease of temperature change, so that an anomaly in the ground surface temperature appears. The thermometer, which trails the heater at a fixed distance, measures the local temperature of the soil surface with a given delay after the heating pulse, and the signal obtained can be easily processed in order to detect such thermal anomaly.

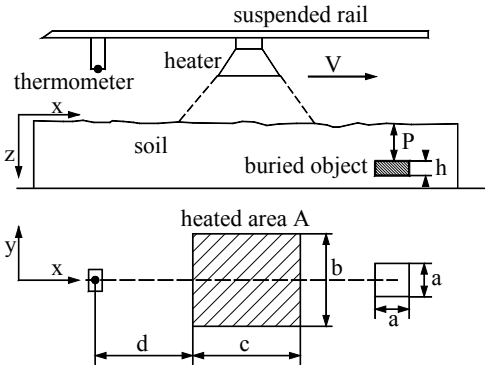

Fig. 1. Sketch of the thermal detector and target geometry.

3 Theoretical model

3.1 Mathematical formulation

An APM, modelled as a parallelepiped of size (a × a × h), with a = 5cm and h = 2cm which correspond to the dimensions of a small APM, is buried at a depth P below the ground surface, as sketched in Fig. 1, where the detection device, and the coordinate system adopted, are also represented. The landmine is supposed to be made of homogeneous material with physical properties similar to those of TNT, i.e., k_m = 0.4 W/mK and $(\rho c)_m = 1.54 \times 10^6$ J/m^{3}K, which give $\alpha_m = 2.6 \times 10^{-7}$ m^2/s, and to lay in a dry, bare soil, with constant physical properties k_s = 0.75 W/mK and $(\rho c)_s = 1.17 \times 10^6$ J/m^{3}K, which give $\alpha_s = 6.4 \times 10^{-7}$ m^2/s.

The heating device, and the trailing thermometer which follows the heater at a given distance d, move at constant velocity V along a scanning line which passes right above the mine. The infrared radiating power is delivered to the ground onto a rectangular area A = b × c, where b and c are the dimensions normal and parallel to the scanning direction, respectively, whose symmetry axis along the scanning direction coincides with the symmetry axis of the projection of the buried landmine upon the ground surface. The contactless thermometer is supposed to read the temperature of the ground surface element located just below the sensor, without any meaningful influence from neighbouring ground elements.

The time-evolution of the temperature field of the ground is calculated through the energy flow equation, under the assumption of homogeneous and isotropic materials:

$$\nabla^2 T = \frac{1}{\alpha_i}\frac{\partial T}{\partial \tau} \quad (i = 1, 2) \tag{1}$$

where subscripts 1 and 2 refer to the soil and to the mine, respectively. The following boundary conditions are used:

a) energy balance at the ground surface, which takes into account the radiant energy absorbed and emitted, the energy exchanged with air by convective heat transfer, and the energy conducted to the soil underneath:

$$a_s W \delta = \sigma \varepsilon (T^4 - T_{mr}^4) + h_c (T - T_a) - k_1 \frac{\partial T}{\partial z} \tag{2}$$

b) heat flux continuity at any soil/mine interface:

$$-k_1 \left.\frac{\partial T}{\partial n}\right|_1 = -k_2 \left.\frac{\partial T}{\partial n}\right|_2 \tag{3}$$

c) zero temperature gradient, i.e., zero heat transfer rate, at the four side-surfaces of the 3D Cartesian integration domain, which are chosen at a sufficiently large distance from the mine:

$$\frac{\partial T}{\partial n} = 0 \tag{4}$$

d) zero temperature gradient, i.e., zero heat transfer rate, at a depth H =1m at which the thermal effects of the soil heating can be neglected, as shown by a series of preliminary tests specifically performed:

$$\left.\frac{\partial T}{\partial z}\right|_{z=H} = 0 \qquad (5)$$

where W is the infrared heating power delivered to the ground surface per unit area; ε is the emissivity of the ground surface in the long-wave IR, which is reasonably assumed equal to 0.9; a_s is the coefficient of absorption of the ground surface in the long-wave IR, which is assumed equal to ε, i.e., 0.9, under the assumption that the soil behaves like a grey-body; δ is a Boolean factor equal to unity or zero, according as the ground surface element being considered is irradiated or not by the heater; σ is the Stefan-Boltzmann constant, equal to 5.67×10^{-8} W/m^2K^4; T_a is the air temperature, which is assumed equal to 20°C along the entire investigation-time; T_{mr} is the ambient mean radiant temperature, assumed equal to T_a under the assumption that the ambient behaves like a black-body; h_c is the coefficient of convection, which, once a wind speed of nearly 2.5m/s is assumed, is taken equal to $15W/m^2K$ [10]; k is the thermal conductivity; and n denotes the direction normal to the surface element being considered.

As far as the initial condition is concerned, i.e., the thermal field across the integration domain at time τ = 0 when the infrared heater starts scanning the ground surface, an initial uniform temperature $T_0 = T_a$ is assumed.

3.2 Numerical simulation

The governing equation (1) with the boundary and initial conditions stated above is solved through a control-volume formulation of the finite difference method. A fully implicit formulation is used for time stepping. Starting from the initial temperature field, at each time-step the discretized governing equation is solved iteratively through a line-by-line application of the Thomas algorithm. Within each time-step, full convergence is assumed when the maximum absolute value of the relative changes of temperature at any grid-node from iteration to iteration is smaller than a prescribed value, i.e., 10^{-6}.

The integration domain, which covers a ground surface of 1.8m × 1.2m and extends down to a depth of 1m, is discretized through a non-uniform grid of more than 1,800,000 nodal points. In particular, an "inner" volume of 80cm × 20cm × 20cm, located just below the ground surface scanned by the detection device and containing the buried object, is filled with equally spaced grid-nodes placed at 0.5cm from each other in the x and y directions, whereas a uniform spatial step of 0.25cm is adopted along the z direction. The remaining of the computational domain is covered by grid-nodes spaced according to a logarithmic distribution. In this way the scanning area is accurately covered by a fine discretization grid, while its surroundings can be extended to a sufficiently large distance, so as to ensure the validity of b.c.'s (4) and (5).

Tests on the dependency of the results obtained on the mesh-spacing, as well as on the dimensions of both the "inner" volume and the whole integration domain, have been systematically performed. The optimal grid-size values, and the optimal extents of the inner volume and of the whole integration domain used for computations (representing a good compromise between solution accuracy and computational time) are such that further grid-refinements or volume-enlargements do not yield for noticeable modifications in the resulting temperature field at assigned sample times.

Simulations are performed for a wide variety of combinations of the values of: (a) the area of the irradiated ground surface A = b × c in the range between $25cm^2$ and $350cm^2$; (b) the aspect ratio of the irradiated ground surface S = c/b, or the ratio R = b/a between the dimension of the irradiated ground surface normal to the scanning direction and the characteristic dimension of the buried landmine, in the ranges between 0.5 and 5, and between 1 and 3, respectively; (c) the burial depth of the landmine P in the range between 1cm and 5cm; (d) the power absorbed at the irradiated ground surface Q = a_s WA in the range between 10W and 10kW; (e) the scanning velocity V in the range between 0.125cm/s and 2.5cm/s; and (f) the delay-time τ_d = d/V, which is the time required to span the distance d between the heated area and the thermometer at the scanning velocity V, in the range between 30s and 2500s.

4 Results and discussion

The results obtained from the numerical simulations carried out show that, after a certain time from the heating pulse, the presence of the buried object creates a disturbance of the temperature field on the ground surface, which may be used to pinpoint its location. By way of example, Fig. 2 shows the time-distributions of the temperature data recorded by the thermometer which follows the heater, and of their time-derivatives, for a given combination of values of P, Q, V, A, and S or R, and for different values of the delay-time τ_d. Time τ which appears in the abscissa is the time elapsed from the beginning of the ground irradiation. The time-derivatives are obtained by means of the angular coefficient of the

line which, instant by instant, interpolates the last five temperature readings.

It may be seen that the disturbance is characterized by a peak of temperature superimposed to a practically uniform distribution, whose height is defined as the "temperature contrast" C induced by the presence of the buried object. The value of C, which is calculated as the maximum difference between the temperature actually recorded by the thermometer and the temperature that would be detected at same location in the absence of buried landmine, is chosen as representative of the detection effectiveness. Of course, also the maximum and the minimum values of the time-derivative of temperature, denoted as $(\partial T/\partial \tau)_{max}$ and $(\partial T/\partial \tau)_{min}$, respectively, may be assumed as useful indicators.

In order to determine how the temperature contrast C depends on the independent variables listed above, i.e., P, Q, V, A, S or R, and τ_d, a parametric analysis has been carried out. The results obtained for R = 1, i.e., b = a = 5cm, will be presented and discussed first.

The distributions of C versus the delay-time τ_d for different values of the scanning velocity V in the range between 0.25cm/s and 2cm/s, are reported in Fig. 3, for, e. g., P = 1cm, Q = 25W, A = 25cm^2, S = 1, and R =1. It may be noticed that the time-distributions of C have a maximum C_{max} at an optimum delay-time $\tau_{d\text{-}opt}$ which is independent of V, and, as expected, the value of C_{max} increases with decreasing the scanning velocity.

The distributions of C versus the delay-time τ_d for different values of the area A of the irradiated ground surface, and of its aspect ratio S at R = 1, in the ranges between 35cm^2 and 100 cm^2, and between 1.4 and 4, respectively, are reported in Fig. 4, for, e. g., P = 2cm, Q = 260W, and V = 0.5cm/s. It may be seen that C is practically independent of the area A of the irradiated ground surface, which implies that the temperature contrast C depends on the radiating power absorbed at the soil surface Q, and not on the radiating power absorbed per unit area q = Q/A.

The distributions of C versus the delay-time τ_d for different combinations of values of Q and V, in the ranges between 25W and 100W, and between 0.25cm/s and 1cm/s, respectively, are reported in Fig. 5, for, e. g., P = 1cm, A = 25cm^2, S = 1, and R =1. As expected, at any value of the scanning velocity, the temperature contrast C increases as the absorbed power Q increases. On the other hand, it is worthwhile noticing that same values of the ratio Q/V give rise to overlapping distributions, the higher is the value of Q/V, the higher is the value of C, which implies that the temperature contrast C is a direct function of Q/V, rather than of Q and V separately, where the ratio Q/V may be interpreted as the energy absorbed by the unit length of the irradiated ground along the scanning direction. Even better, since all the results reported in Fig. 5 have been obtained at a constant value of b, i.e., 5cm, the correlation between C and Q/V may be replaced by a correlation between C and (Q/V)/b. Thus, C may conveniently be expressed by a function of such new parameter e = (Q/V)/b, which represents the energy absorbed by the unit area of the irradiated ground. As regards the type of function, the distributions of C versus e for, e. g., P = 1cm, S =1, R =1, and delay-times 90s and 210s, are reported in Fig. 6, where a substantially linear dependency of C from e may be noticed.

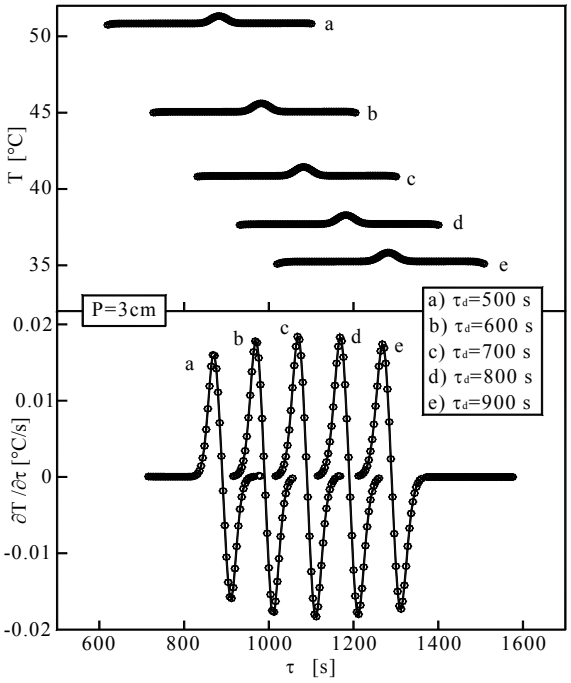

Fig. 2. Thermometer readings and their time-derivatives for different values of τ_d (P=1cm, Q=100W, V=0.25cm/s, S=1, and R=1).

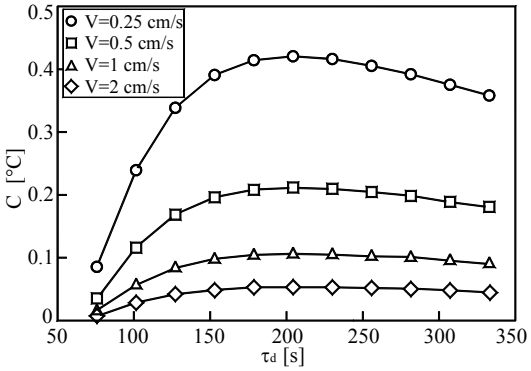

Fig. 3. Distributions of C vs. τ_d for different values of V (P=1cm, Q=25W, S=1, and R=1).

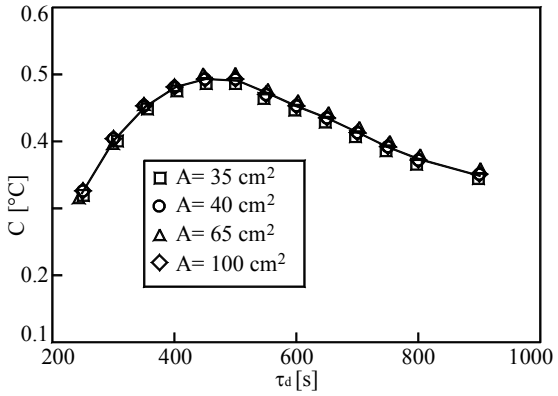

Fig. 4. distributions of C vs. τ_d for different values of A (P=2cm, Q=260W, V=0.5cm/s, and R=1).

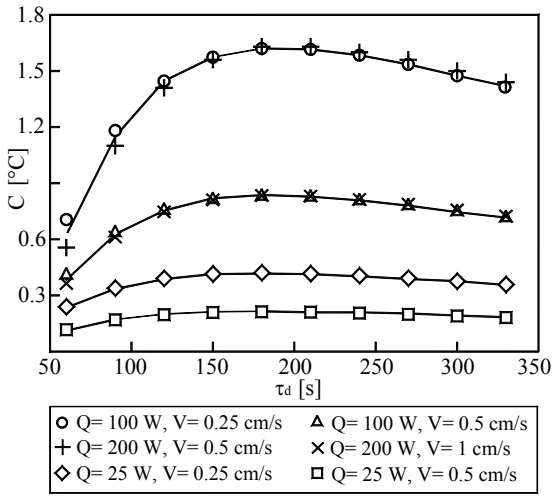

Fig. 5. Distributions of C vs. τ_d for different values of the pair Q-V (P=1cm, S=1, and R=1)

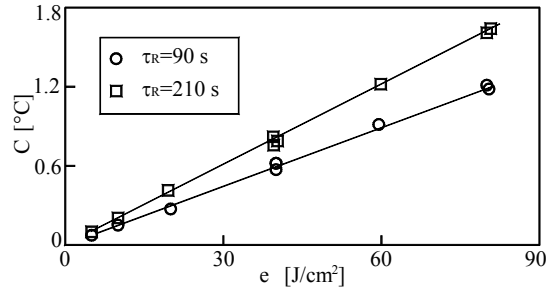

Fig. 6. Distributions of C vs. e for different values of τ_d (P=1cm, S=1, and R=1).

Same type of results have been obtained for any other combination of values of P and S.

Finally, the effects of the burial depth P on the effectiveness of the detection device are highlighted in Fig. 7, where the distributions of C versus τ_d for different values of P in the range between 1cm and 5cm are represented for, e. g., e = 750 J/cm^2, and R =1. It may be noticed that, once the intensity of the thermal stimulation is assigned, the temperature contrast increases, and the optimum delay-time decreases, as the burial depth decreases.

According to what has been illustrated above for the case R = 1, the dependency C = f (P, Q, V, A, S, τ_d) may be reduced to C = f (P, e, τ_d), which, once the attention is reasonably focused upon C_{max}, which occurs at $\tau_{d\text{-}opt}$, leads to C_{max} = f (P, e).

The results obtained from nearly 100 numerical simulations performed for R =1 (that is, b = a = 5cm), $1 \le S \le 5$, $1\text{cm} \le P \le 5\text{cm}$, $1\text{J/cm}^2 \le e \le 2100\text{J/cm}^2$, $0.1°\text{C} < C_{max} < 1.5°\text{C}$, $10\text{W} \le Q \le 1000\text{W}$, $12000\text{W/m}^2 \le q = Q/A \le 85000\text{W/m}^2$, and $0.125\text{cm/s} \le V \le 2.5\text{cm/s}$, are summarized in Fig. 8, where the distributions of C_{max} vs. e are represented for different values of the burial depth P.

It may be noticed that, at least for R =1 and within the aforementioned ranges of investigation, C_{max} is a practically linear function of e, i.e., C_{max} = F(P) × e, where F(P) may be well represented through a decreasing exponential function, as shown in Fig. 9, in which the distribution of C_{max}/e versus P is reported.

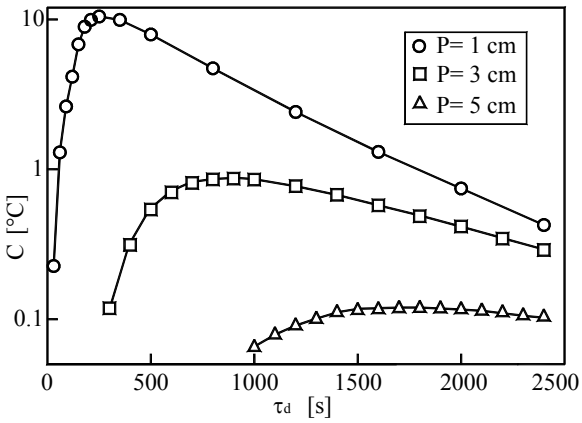

Fig. 7. Distributions of C vs. τ_d for different values of P (e=750J/cm^2, and R=1).

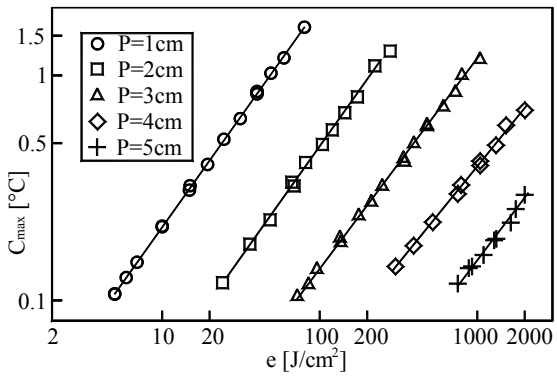

Fig. 8. Distributions of C_{max} vs. e for different values of P (R=1).

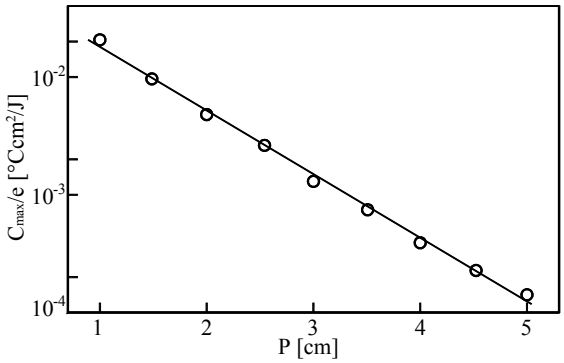

Fig. 9. Distributions of C_{max}/e vs. P (R=1).

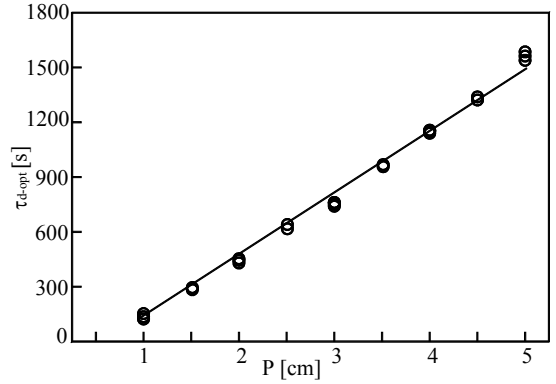

Fig. 10. Numerical values of $\tau_{d\text{-}opt}$ plotted vs. P (R=1).

As concerns the optimum delay-time at which C_{max} occurs, the values obtained for all the geometric-thermal configurations investigated are summarized in Fig. 10, where $\tau_{d\text{-}opt}$ proves to be a substantially linear function of the only burial depth P.

The analysis conducted up to now, performed for R = 1, has then been extended to situations with different values of R, i.e., R = 2 and R = 3, leading to same type of results, i. e., a linear dependency of C_{max} on e at the several burial depths investigated, an exponential dependency of C_{max}/e from P, and a linear dependency of $\tau_{d\text{-}opt}$ from P. In this regard, denoted C^1_{max} as the value of C_{max} corresponding to R = 1, the distributions of the ratio C_{max}/C^1_{max} versus R, for different combinations of values of P and e ranging between 2cm and 5cm, and between 36 J/cm^2 and 1280 J/cm^2, respectively, are reported in Fig. 11. It may be noticed that, for any given value of P, C_{max} increases with R. In fact, the area of the irradiated ground surface around the mine increases with increasing b, which contributes to improve the temperature contrast. On the other hand, as b becomes much greater than a, the irradiation of the peripheral portions of the scanned ground surface is no longer useful to the mine detection, which accounts for the asymptotic increase of C_{max} with R. This is shown also in Fig. 12, where the linear distributions of C_{max} versus e for, e.g., P=5cm, are represented for increasing values of R. Of course, the deeper the mine is buried, the larger is the area of the irradiated ground surface which contributes to the formation of the temperature contrast, and thus the larger is the value of the ratio R = b/a which is convenient to employ. Of course, in order to keep a given value of e, whenever R is increased, also the ratio Q/V has to be correspondingly increased, which means to enhance Q and/or reduce V.

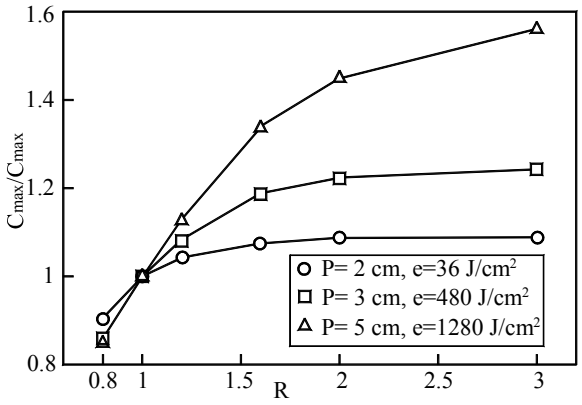

Fig. 11. Distributions of C_{max}/C^1_{max} vs. R for different values of the pair P-e.

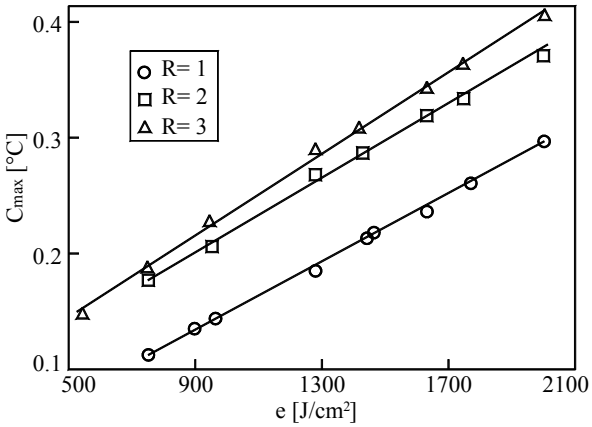

Fig. 12. Distributions of C_{max} vs. e for different values of R (P = 5cm)

In order to give an example of application, consider the urgence to localize a mine 5cm across, down to a maximum burial depth P = 5cm, which is the depth below the ground surface within which the IR thermal detection methods have the objective of revealing the presence of mine candidates. Let us assign C_{max} = 0.3°C, and assume R = b/a = 2. From the data reported in Fig. 12, an absorbed energy per unit area e = 1500 J/cm^2 is required. If the scanning velocity V is, e. g., chosen equal to 0.25cm/s, the power which is required to be absorbed at the soil surface is Q = e × V × b = 3.25kW. Once $a_{s\text{-}IR}$ = 0.9 and no radiating power losses are assumed, this

corresponds to a 3.6kW power of the detection device. The area of the ground surface which is scanned per unit time is $V \times b = 2.5cm^2/s = 0.9 m^2/h$, which means that $1m^2$ of soil surface is scanned in little more than one hour. In addition, according to Fig. 12, the optimum delay-time $\tau_{d\text{-}opt}$ is of the order of 1500s, which would suggest the advisability of adopting two separate scanning devices, one for the heater, and another one for the thermometer.

5 Conclusions

The possibility of detection of small anti-personnel landmines buried at depths between 1cm and 5cm in a homogeneous ground with a bare, flat surface by means of an active scanning device basically consisting of an infrared focused heater and a trailing contactless thermometer, has been studied numerically through a specifically developed computer-code.

The main results obtained may be summarized as follows:

(a) Some time after the ground irradiation, the presence of the hidden object gives rise to a disturbance in the surface temperature, whose time-distribution shows a maximum at an optimum delay-time, which depends only on the burial depth of the landmine.

(b) The maximum temperature contrast has a substantially linear dependency on the energy absorbed by the unit area of the irradiated ground surface.

(c) The ratio between the maximum temperature contrast and the energy absorbed per unit area of the irradiated ground surface decreases exponentially with increasing the burial depth of the landmine, which implies that, once a minimum value of the detectable temperature contrast is assigned**,** the energy required to produce such contrast increases exponentially with the burial depth.

(d) The maximum temperature contrast increases asymptotically as the ratio between the dimension of the irradiated ground surface normal to the scanning direction and the characteristic dimension of the mine increases.

(e) In addition to the temperature readings, also their time-derivative may be used as a further helpful information. In fact, in correspondence of the buried object such derivative has a positive peak followed by a negative one, whose amplitudes are several orders of magnitude greater than the values typical for the undisturbed situation.

Within the bounds of the numerical simulations executed and the approximation introduced, typical for a first-approach study, the results obtained prove the feasibility of the device, whose main advantage is its simplicity, as it is based on cheap, sturdy, and easily serviceable hardware, and gives simple readings to the operator.

Nevertheless, it seems essential to take into due account that both the non-homogeneity of real soils and real climatic conditions, i.e., solar irradiation and air temperature changes during the investigation-time, may produce non-negligible effects on the ground surface temperatures, which will be the object of the second part of the present work.

References:

[1] Bruschini, K. De Bruyn, H. Sahli, J. Cornelis, Study on the state of the art in the EU related to humanitarian demining technology, products and practice, EUDEM: EU in humanitarian DEMining final report, (1999).

[2] J. T. Broach, R. S. Harmon, G. J. Dobeck (eds.), Detection and remediation technologies for mines and minelike targets VII, Proceedings of the SPIE, vol. 4742 (2002).

[3] P. Li, A. Maad, F. Moshary, M. F. Arend, S. Ahmed, Infrared imaging of buried objects by thermal step-function excitations, Applied Optics 34 (1995) 5809-5816.

[4] S. Sjökvist, M. Uppsäll, S. Nyberg, A. Linderhed, M. Lundberg, Optical detection of land mines at FOI, Proceedings of the SPIE, vol. 4491 (2001).

[5] K. Khanafer, K. Vafai, Thermal analysis of buried land mines over a diurnal cycle, IEEE Transactions on Geoscience and Remote Sensing 40 (2002) 461-473.

[6] S. M. Khanna, F. Paquet, R. G. Apps, J. S. Seregelyi, Landmine detector with a high-power microwave illuminator and an infrared detector, U.S. Patent no. 6,343,534 (2002).

[7] P. López, D. L. Vilariño, D. Cabello, H. Sahli, M. Balsi, CNN-based 3D thermal modeling of the soil for antipersonnel mine detection, CNNA 2002, Proceedings of the 7th IEEE international workshop on cellular neural networks and their applications (2002) 307-314.

[8] P. López, L. van Kempen, H. Sahli, D. C. Ferrer, Improved thermal analysis of buried landmines, IEEE Transactions on Geoscience and Remote Sensing 42 (2004) 1965-1975.

[9] M. Balsi, M. Corcione, Thermal detection of buried landmines by local heating, International Journal of Systems Science 36 (2005) 589-604.

[10] W. C. Mc Adams, Heat transmission, 3rd ed., Mc Graw-Hill, New York, 1954.